Role of Laser-Induced Plasma Formation in Pulsed Cellular Microsurgery and Micromanipulation

Vasan Venugopalan,[1,2,3,*] Arnold Guerra III,[1,2] Kester Nahen,[4] and Alfred Vogel[4,†]

[1]*Department of Chemical Engineering and Materials Science, University of California, Irvine, California 92697-2575*
[2]*Laser Microbeam and Medical Program, Beckman Laser Institute, University of California, Irvine, California 92612-3010*
[3]*Center for Biomedical Engineering, University of California, Irvine, California 92697-2715*
[4]*Medical Laser Center Lübeck, Peter Monnik Weg 4, D-23562 Lübeck, Germany*

(Received 20 June 2001; published 4 February 2002)

We investigate experimentally the physical processes underlying pulsed cellular microsurgery and micromanipulation using nanosecond 532- and 1064-nm laser pulses focused at high numerical aperture. We find that the laser parameters employed for many microirradiation techniques are congruent with those leading to optical breakdown in water. We determine the size and shape of the laser-induced plasma, pressure of the emitted shock wave, and size and energy of the cavitation bubble formed by the expanding plasma. We discuss implications of the results for biophysical microirradiation procedures.

DOI: 10.1103/PhysRevLett.88.078103 PACS numbers: 87.80.–y, 42.62.–b, 52.50.–b, 87.50.–a

The use of highly focused pulsed laser irradiation to modify and manipulate biological media for applications in molecular and cellular biophysics and biotechnology becomes more pervasive with each passing year [1]. Currently, such procedures enable the dissection or inactivation of cellular organelles, cytoskeletal filaments, and chromosomes with submicron spatial precision [2]. Microirradiation procedures are also used to deliver genes or biomolecules via transient permeabilization of the plasma cell membrane. Permeabilization can be achieved in multiple cells via a process known as optoporation or in a single cell via a process known as optoinjection [3–5]. Most recently, pulsed lasers have enabled the sampling and subsequent biophysical characterization of cellular structures using laser pressure catapulting [6]. Remarkably, while pulsed laser microbeam technologies continue to advance, the physical mechanisms that enable them have rarely been studied [7,8] and for all practical purposes remain an enigma. Knowledge of these physical mechanisms is of vital importance and would provide a framework wherein novel and improved laser microbeam techniques can be developed and the systematic investigation of novel pulsed microbeam effects pursued.

The precise modification of cellular structures achieved by laser microirradiation suggests that energy deposition is accomplished on a submicron spatial scale. The fact that these techniques often employ visible and near infrared wavelengths, a region in the optical spectrum where little linear absorption by endogenous biomolecules is present, suggests that nonlinear optical phenomena are operative. In our view, the primary candidate mechanism responsible for the observed effects is laser-induced plasma formation (optical breakdown), because the laser parameters typically employed generate irradiances $\geq 10^8$ W/mm^2 and are known to produce quasifree electrons via multiphoton and/or cascade ionization [9].

To confirm this hypothesis, we performed experiments using nanosecond pulsed laser irradiation of water focused at high numerical apertures. We determined the threshold for plasma formation, measured the plasma size and shape, and investigated the shock wave propagation and cavitation bubble dynamics driven by the expanding plasma. Distilled water was used since optical breakdown in water is similar to that in ocular and other transparent biological media [10].

Figure 1 depicts the experimental setup. The 1064- or 532-nm output of a Q-switched Nd:YAG laser entered the rear aperture of a 63×, 0.9 numerical aperture (NA), water-immersion microscope objective (Leica HCX APO L U-V-I) via a dichroic beam splitter (high reflectivity at $\lambda = 1064$ nm; ~50% reflectivity in the visible). The microscope objective was built into the wall of a water-filled, quartz cuvette to enable delivery of a single 6-ns "pump" pulse without the corrupting effects of optical aberrations known to perturb the optical breakdown process [11]. Imaging of the plasma and subsequent hydrodynamics was enabled by two 35-mm cameras. A view along the optical axis with 30× magnification was obtained by

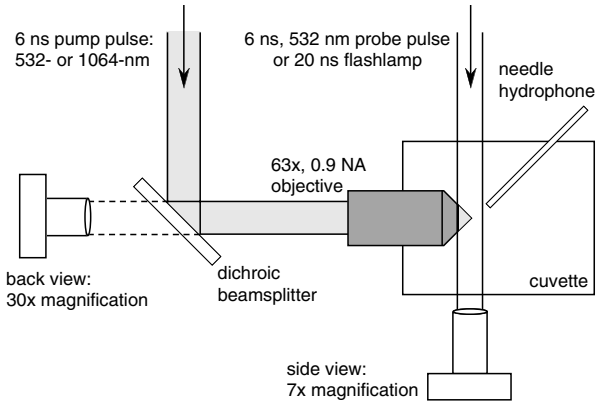

FIG. 1. Experimental setup used for the examination of laser-induced breakdown of water. The pump laser beam entering the rear aperture of the microscope objective has a uniform irradiance distribution.

fitting a camera with a 105-mm lens and placing it behind the dichroic beam splitter. A side view was provided by a second camera fitted with a 7× lens (Leitz Photar). The energy of each pump laser pulse was measured by a pyroelectric detector.

The shock wave dynamics were photographed by transilluminating the volume surrounding the focus with a 6-ns "probe" pulse of 532-nm radiation from the Nd:YAG laser at a time delay relative to the pump pulse. An optical delay line provided delays of 0 to 32 ns between the pump and probe pulses. To visualize the cavitation bubble dynamics, we used an ultrashort duration (<20 ns) flashlamp triggered by a timed electronic delay. Moreover, a polyvinylidene fluoride needle hydrophone (Ceram) with a rise time of 12 ns and a 1-mm^2 active area was placed 10 mm above the focal volume to measure the acoustic emission produced by the shock wave and subsequent cavitation dynamics.

The threshold energy for plasma formation was determined by delivering 20 laser pulses of fixed energy to the water-filled cuvette in a dark room. The number of pulses resulting in plasma formation, as determined by the appearance of a visible flash, was recorded. This procedure was repeated for 20 pulse energies and the probability of plasma formation versus pulse energy was plotted and fit to a Gaussian error function [12]. From this fit, the energy for a 50% probability of plasma formation was determined to be 1.89 and 18.3 μJ for 532- and 1064-nm irradiation, respectively, and denoted as the energy threshold E_{th} for plasma formation. Assuming diffraction limited conditions, such pulse energies correspond to threshold irradiances I_{th} of 0.77×10^9 and 1.87×10^9 W/mm^2 for 532- and 1064-nm irradiation, respectively. These threshold values are remarkably similar to the laser parameters employed in optoinjection [5]. Specifically, when using an oil-immersion microscope objective with NA = 1.3, optoinjection is achieved at threshold pulse energies of 0.5 and 12 μJ for 532- and 1064-nm irradiation, respectively, and correspond to threshold irradiances of 0.51×10^9 and 3.1×10^9 W/mm^2.

We photographed the plasma using pump pulse energies E_p of 1×, 2×, 5×, and 10× threshold. The plasma was ellipsoidal in shape, appearing elliptical in the side view and circular in the back view. Table I lists the plasma length l as measured from the side view, diameter d as measured from the back view, and plasma volume V_p ($= \pi d^2 l/6$) for the various pulse energies and irradiation wavelengths. At threshold, the plasma volume for 532- and 1064-nm radiation, was 9.97 and 581 μm^3, respectively. Assuming diffraction limited conditions, we define the focal volume as a cylinder with a diameter equaling that of the laser spot $d = 1.22\lambda/\text{NA}$ and length equaling 2 times the Rayleigh range $z_R = \pi d^2/4\lambda$. The plasma volume created at threshold is larger than the focal volume by factors of 16.3 and 117 for 532- and 1064-nm irradiation, respectively.

TABLE I. Plasma dimensions and their variation with pulse energy.

Wavelength λ [nm]	Normalized pulse energy $\beta = (E_p/E_{\text{th}})$	Plasma length l [μm]	Plasma diameter d [μm]	Plasma volume V_p [μm^3]
1064	1	14.0	8.9	581
1064	2	25.0	15.5	3140
1064	5	37.9	21.0	8750
1064	10	47.3	27.5	18 700
532	1	3.6	2.3	9.97
532	2	3.8	2.9	16.7
532	5	8.4	5.1	114
532	10	12.6	7.6	381

The larger size of the plasma relative to the focal volume is due to luminescence emitted by the plasma during its expansion. When the plasma begins to form, electron-hole recombination results in emission of UV radiation. These high energy photons contribute to the formation of additional quasifree electrons in the plasma vicinity that in turn act as seed electrons for cascade ionization. Optical breakdown will occur wherever the local irradiance is sufficient to produce an electron density corresponding to a luminescent plasma. The lower photon energy provided by 1064-nm radiation demands that a higher irradiance be used to generate the initial quasifree electrons in the conduction band through multiphoton ionization compared to that required to complete the cascade ionization process [9]. This higher irradiance threshold is responsible for both the higher pulse energy threshold and the larger plasma size generated by 1064- vs 532-nm irradiation.

Time-resolved photography was used to determine the variation of the shock wave propagation speed with distance r from the plasma center. This was used in conjunction with the equation of state for water [13] to determine the peak pressure p_S of the shock wave as a function of r

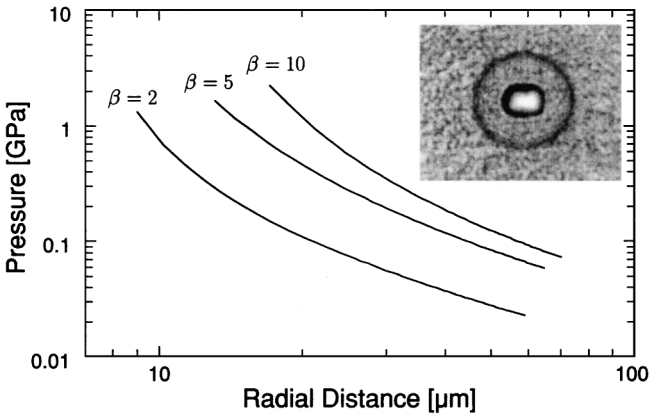

FIG. 2. Shock wave pressure vs propagation distance generated by 1064-nm irradiation for pulse energies 2×, 5×, and 10× threshold. Inset: plasma, shock wave, and cavitation bubble photographed 30 ns after delivery of a 1064-nm pump pulse at 10× threshold energy.

TABLE II. Shock wave and cavitation bubble dynamics parameters in water for 532- and 1064-nm irradiation. These include the pump pulse energy E_p, shock wave pressure at 10 mm from the optical breakdown site p_S, temporal width of the pressure transient at the half maximum level Δt_S, shock wave energy at 10 mm from the optical breakdown site E_S, cavitation bubble oscillation period T_{osc}, maximum bubble radius R_{max}, and bubble energy E_B.

λ [nm]	β	E_p [μJ]	p_S [MPa]	Δt_S [ns]	E_S [μJ]	E_S/E_p [%]	T_{osc} [μs]	R_{max} [μm]	E_B [μJ]	E_B/E_p [%]
1064	1	18.0 ± 0.1	0.158 ± 0.028	42.0 ± 0.5	0.64	3.6	27.7	151.3	1.45	9.1
1064	2	36.4 ± 0.2	0.283 ± 0.008	47.5 ± 1.0	2.33	6.4	45.3	247.6	6.35	17.3
1064	5	90.9 ± 0.3	0.475 ± 0.009	53.0 ± 0.5	7.32	8.1	65.9	360.1	19.57	21.5
1064	10	182.2 ± 0.9	0.659 ± 0.005	59.0 ± 0.5	15.69	8.6	86.6	473.3	44.41	24.4
532	1	1.89 ± 0.10	0.038 ± 0.008	26.0 ± 0.5	0.023	1.2	8.3	45.4	0.039	2.1
532	2	3.78 ± 0.13	0.091 ± 0.005	31.0 ± 0.5	0.157	4.2	13.8	75.4	0.180	4.2
532	5	9.19 ± 0.30	0.202 ± 0.008	36.0 ± 0.5	0.90	9.8	26.9	147.0	1.33	14.3
532	10	19.15 ± 0.60	0.310 ± 0.001	43.0 ± 0.5	2.53	13.2	37.5	205.0	3.60	19.3

[14]. Such $p_S(r)$ curves are shown in Fig. 2 along with a photograph of the shock wave. These plots begin at a distance corresponding to the plasma size reported in Table I. Thus the maximum pressure of each curve represents the pressure at the plasma rim. For 1064-nm irradiation this pressure ranges from 1.3 GPa for pulse energies 2× threshold to 2.2 GPa for pulse energies 10× threshold.

Table II displays the results pertinent to shock wave propagation at larger distances and cavitation bubble dynamics. Shock wave pressure p_S and duration Δt_S refer to a distance $r_S = 10$ mm from the focal volume. Assuming that the temporal profile of the shock wave pressure (shown in Fig. 3) is well approximated by an exponential pulse with a full width at half maximum Δt_S equal to that given by the hydrophone measurements, the energy of the shock wave of radius r_S is given by [15]

$$E_S(r_S) = 6.124 \times 10^{-9} p_S^2 r_S^2 \Delta t_S\,, \qquad (1)$$

where the shock wave energy E_S is given in μJ, shock wave peak pressure p_S in MPa, shock wave radius r_S in μm, and Δt_S in ns. The shock wave energy, as well as the ratio of shock wave energy to laser pump pulse energy (E_S/E_p), is listed in Table II. Note that the shock wave energy calculated at $r_S = 10$ mm represents only about 10%–15% of the initial shock wave energy because significant dissipation occurs during its near-field propagation [15]. Nevertheless, (E_S/E_p) is a measure of the conversion efficiency of laser pulse energy into mechanical energy and also indicative of the energy density of the plasma. The results in Table II show that, for equivalent normalized pulse energies $\beta = (E_p/E_{\text{th}})$, conversion of laser pulse energy into shock wave energy is smaller for 532- than for 1064-nm irradiation at $\beta \leq 2$, while for $\beta > 2$ the conversion is larger for 532-nm irradiation. However, given the significantly smaller value for E_p, the absolute value for E_S is still much smaller for 532-nm irradiation even at large β. These findings are consistent with the observation that pulsed microbeam effects achieved using 1064-nm irradiation tend to be more violent and less precise than those achieved using 532-nm irradiation.

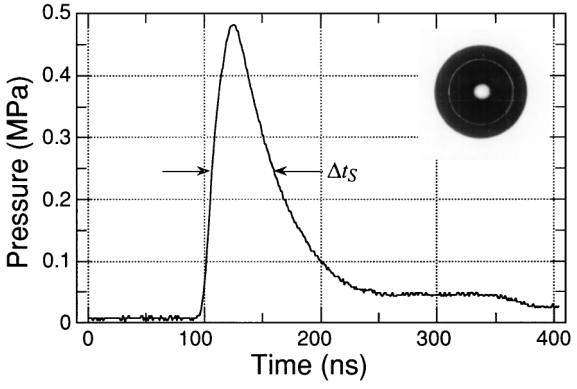

FIG. 3. Temporal profile of shock wave pressure generated by 1064-nm irradiation at 5× threshold energy measured 10 mm from the optical breakdown site. Inset: cavitation bubble of 720 μm diameter formed by a 1064-nm pump pulse at 5× threshold energy.

On the microsecond time scale, the hydrophone data exhibit pressure transients originating from optical breakdown and cavitation bubble collapse and provide direct measurement of the bubble oscillation period T_{osc}. The oscillation period is related to the maximum bubble radius R_{max} via the Rayleigh formula [14] and enables determination of the bubble energy E_B using the relation [14]

$$E_B = \frac{4}{3}\,\pi \rho_0 \left(\frac{2 \times 0.915}{T_{\text{osc}}}\right)^2 R_{\text{max}}^5\,, \qquad (2)$$

where ρ_0 is the mass density of the unperturbed water.

Values of the bubble energy, and of the ratio of cavitation bubble energy to the incident laser pulse energy (E_B/E_p), are listed in Table II. For a given β, the transduction of laser pulse energy to bubble energy is more efficient at 1064- than at 532-nm irradiation. The large cavitation bubble radii confirmed by our photographic studies (Fig. 3, inset) are a bit perplexing. We find that, at the breakdown threshold, the maximum bubble radius is 45 and 150 μm for 532- and 1064-nm irradiation, respectively. At first glance this does not appear consistent with the fact that modification of biological media using pulsed microbeams

is achieved with submicrometer resolution. However, it must be noted that expansion of cavitation bubbles in water is much larger than in tissue and biological media due to greater viscosity/stiffness of the cytoplasm and cytoskeleton. For example, cavitation bubbles formed via optical breakdown in corneal stroma for a given pulse energy are only a third of the diameter (1/27th the volume) of those created in water [16]. Moreover, when the plasma is produced at the cell membrane surface as in optoinjection, the bubble will expand mainly into the extracellular space and cause less deformation of the cytoskeleton than when the pulse is delivered to the cell interior. Nevertheless, the large bubble diameters remain a matter of concern, and direct visualization will be necessary to resolve precisely how cells are perturbed by the physical transients generated by pulsed laser microbeam irradiation.

Our results indicate that cavitation and shock wave dynamics are also the working mechanism for optoporation; a procedure wherein transient membrane permeabilization and molecular delivery is achieved in several cells via delivery of a single focused laser pulse of larger energy to a location within a cell culture at a distance from the cells of interest. Soughayer and co-workers observed that optoporation is achieved without loss of cell viability in a zone 30–60 μm from the laser focus using 10 μJ pulses of 532-nm radiation [3]. Extrapolation of the far-field data shown in Table II for 532-nm irradiation at $E_p = 9.2$ μJ ($\beta = 5$) indicates that cells in this region are subjected to pressures between 46 MPa at 60 μm and 96 MPa at 30 μm. Pressures of similar magnitude were also obtained in this region in our near-field measurements for 1064-nm irradiation (Fig. 2).

In conclusion, our results implicate laser-induced plasma formation as the primary mechanism enabling pulsed cellular microsurgery and micromanipulation. The energy and irradiance thresholds for this process are congruent with threshold laser parameters used for optoinjection. Moreover, the threshold pulse energy and transduction of laser pulse energy to cavitation bubble energy is significantly higher at 1064-nm irradiation compared to 532-nm irradiation. These findings are also consistent with characteristics of pulsed cellular microsurgery where it is known that subtle manipulations and fine lesions are more easily achieved and controlled using 532- as opposed to 1064-nm irradiation [5]. From the finding that optical breakdown is the working mechanism of pulsed cellular microsurgery we can deduce that a refinement of laser effects may be achieved by employing laser pulses with shorter durations as it is known that the energy threshold for optical breakdown decreases strongly with decreasing pulse duration [9,12].

We acknowledge support from the Laser Microbeam and Medical Program (NIH-P41-RR-01192), Bioengineering Research Partnership Program (NIH-R01-RR-14892), the German Research Foundation (DFG, Grant No. Bi321/2-4), and the School of Engineering at UC Irvine. Experiments were performed at the Medical Laser Center, Lübeck, Germany.

*Corresponding address: Department of Chemical Engineering and Materials Science, 916 Engineering Tower, University of California, Irvine, California 92697-2575.
Email address: vvenugop@uci.edu
†Email address: VOGEL@mll.mu-luebeck.de

[1] K. O. Greulich, G. Pilarczyk, A. Hoffmann, G. M. Z. Hörste, B. Schäfer, V. Uhl, and S. Monajembashi, J. Microsc. **198**, 182 (2000).
[2] M. W. Berns, W. H. Wright, and R. W. Steubing, Int. Rev. Cytol. **129**, 1 (1991).
[3] J. E. Soughayer, T. B. Krasieva, S. C. Jacobson, J. M. Ramsey, B. J. Tromberg, and N. L. Allbritton, Anal. Chem. **72**, 1342 (2000).
[4] W. Tao, J. Wilkinson, E. J. Stanbridge, and M. W. Berns, Proc. Natl. Acad. Sci. U.S.A. **84**, 4180 (1987).
[5] T. B. Krasieva, C. F. Chapman, V. J. Lamorte, V. Venugopalan, M. W. Berns, and B. J. Tromberg, Proc. SPIE Int. Soc. Opt. Eng. **3260**, 38 (1998).
[6] K. Schütze and G. Lahr, Nat. Biotechnol. **16**, 737 (1998).
[7] M. W. Berns, Biophys. J. **16**, 973 (1976).
[8] P. P. Calmettes and M. W. Berns, Proc. Natl. Acad. Sci. U.S.A. **80**, 7197 (1983).
[9] J. Noack and A. Vogel, IEEE J. Quantum Electron. **35**, 1156 (1999).
[10] F. Docchio, C. A. Sacchi, and J. Marshall, Lasers Ophthalmol. **1**, 83 (1986).
[11] A. Vogel, K. Nahen, D. Theisen, R. Birngruber, R. J. Thomas, and B. A. Rockwell, Appl. Opt. **38**, 3636 (1999).
[12] A. Vogel, K. Nahen, D. Theisen, and J. Noack, IEEE J. Sel. Top. Quantum Electron. **2**, 847 (1996).
[13] M. H. Rice and J. M. Walsh, J. Chem. Phys. **26**, 824 (1957).
[14] A. Vogel, S. Busch, and U. Parlitz, J. Acoust. Soc. Am. **100**, 148 (1996).
[15] A. Vogel, J. Noack, K. Nahen, D. Theisen, S. Busch, U. Parlitz, D. X. Hammer, G. D. Noojin, B. A. Rockwell, and R. Birngruber, Appl. Phys. B **B68**, 271 (1999).
[16] A. Vogel, M. R. C. Capon, M. N. Asiyo-Vogel, and R. Birngruber, Invest. Ophthalmol. Visual Sci. **35**, 3032 (1994).